ISSN 0023-1584, Kinetics and Catalysis, 2010, Vol. 51, No. 6, pp. 832–842. © Pleiades Publishing, Ltd., 2010.
Original Russian Text © V.A. Nasluzov, E.A. Ivanova-Shor, A.M. Shor, I.V. Yudanov, N. Rösch, 2010, published in Kinetika i Kataliz, 2010, Vol. 51, No. 6, pp. 859–870.

## VIII INTERNATIONAL CONFERENCE ON MECHANISMS OF CATALYTIC REACTIONS

# Simulation of Heterogeneous Catalysts and Catalytic Processes Using the Density Functional Method

**V. A. Nasluzov[a], E. A. Ivanova-Shor[a], A. M. Shor[a], I. V. Yudanov[b], and N. Rösch[c]**

[a] *Institute of Chemistry and Chemical Technology, Siberian Branch, Russian Academy of Sciences, Krasnoyarsk, 660049 Russia*
[b] *Boreskov Institute of Catalysis, Siberian Branch, Russian Academy of Sciences, Novosibirsk, 630090 Russia*
[c] *Technical University of Munich, D-85747 Garching, Germany*
*e-mail: as@icct.ru, ilya@catalysis.ru, roesch@ch.tum.de*

Received November 16, 2009

**Abstract**—The review is devoted to the use of high-level quantum-chemical calculations by the density functional method for the simulation of heterogeneous catalytic systems based on transition metals. The following problems are considered: (1) the development of methods for simulating metal particles supported on the surfaces of ionic and covalent oxides; (2) the calculation of the properties of individual transition metal atoms and small clusters adsorbed on the surfaces of MgO, $\alpha$-$Al_2O_3$, $\gamma$-$Al_2O_3$, and various modifications of $SiO_2$ and in the pores of zeolites; (3) the mechanisms of hydrogen activation and acrolein hydrogenation on the metallic and partially oxidized surface of silver; and (4) the mechanism of formation of carbon residues upon the decomposition of methanol on nanosized Pd particles.

**DOI:** 10.1134/S0023158410060091

## INTRODUCTION

The state-of-the-art methods of computer chemistry make it possible to simulate real catalysts and catalytic systems with a sufficient accuracy. Because of increasing accuracy and reliability, theoretical methods became a powerful tool for studying complex chemical processes on the surfaces of heterogeneous catalysts. The results of quantum-chemical calculations can currently supplement experimental data and facilitate their adequate interpretation. This review demonstrates recent achievements in studying various types of solid catalysts by the density functional (DF) method. In particular, the simulation of small metal clusters on oxide surfaces and in zeolite cavities and the calculations of chemical reactions on the surfaces of metals and nanosized metal particles are considered. The reported studies were performed in close collaboration of the group of theoretical chemistry at the Technical University of Munich and the quantum chemistry groups at the Institute of Chemistry and Chemical Technology (Krasnoyarsk) and the Boreskov Institute of Catalysis (Novosibirsk). The knowledge accumulated in more than 15 years of collaboration allowed us to develop an original procedure for simulating the oxide environment of a cluster model specially adapted to precisely describe various particles immobilized on oxide supports, including atoms and metal clusters.

The review consists of the following sections: The first section is devoted to the construction and main characteristics of the procedure developed for the introduction of a cluster into an elastic polarizable environment (EPE). Attention is focused on differences in the simulation of adsorption on ionic and polar covalent oxides. The next section considers the studies of small metal particles on oxide substrates performed with the use of an EPE model. The final section describes the calculations of acrolein hydrogenation reactions on the surface of silver and the mechanism of C–O bond cleavage in the course of methanol decomposition on nanosized palladium particles.

## EPE METHOD: EMBEDDING A CLUSTER IN AN ELASTIC POLARIZABLE ENVIRONMENT

Cluster embedding methods, that is, methods for the approximate description of a crystalline environment of cluster surface models, are widely used in the quantum-chemical calculations of solid surfaces and adsorption complexes [1]. In the general case, the environment of a cluster model is described by a less accurate method than the cluster, which is of the greatest interest in terms of its chemical and physical properties. The results of the calculations of embedded cluster models essentially depend on the size and shape of a region to be quantum chemically described and on the approximation level used to describe the surrounding space of the quantum-mechanical part of the model. We developed a highly accurate method of cluster embedding in an elastic polarizable environment (EPE) and practically implemented it in the ParaGauss quantum-chemical program package oriented to DF calculations [2].

The scheme of the EPE method is the following: (i) a regular (defectless) surface is described by a periodic two-dimensional model (slab) and calculated by molecular mechanical (MM) methods; (ii) an active site of the regular surface is described by a quantum-mechanical (QM) cluster embedded in the MM slab represented as an EPE; (iii) a test surface site, defect, or surface complex is considered as a disturbance in the regular periodic structure; (iv) two types of interactions between QM and MM parts—long-range (electrostatic) and short-range interactions, which contribute to the total energy of the system—are introduced; and (v) the ground state of the entire system is calculated variationally by minimizing the total energy [3].

Thus, the test system in the EPE method is subdivided into two parts. Region I includes an active site, and it is a QM cluster. Region II includes a crystalline environment, which is described by the EPE method. A shell model is used to take into consideration electronic polarization effects, and the Mott–Littleton approximation is also used in the case of a charged defect [4, 5]. The direct insertion of a QM cluster into an environment whose atomic centers are modeled by point charges leads to an artificial distortion in the electron density of anions in region I, which directly contact with positive point charges in region II. The EPE method is free of such distortions to a large extent; it replaces point charges at the boundary between regions by cationic model potentials. The interface thus formed between regions I and II is incorporated into a QM cluster as effective potentials (pseudopotentials (PPs)).

In the EPE method, the total energy ($E_{tot}$) of the entire system is calculated as the sum of the three contributions that describe interactions within a QM cluster ($E_{cl}$), between the QM cluster and the environment ($E_{int}$), and within the surrounding crystal lattice ($E_{lat}$). The effect of region II on region I is represented by the Madelung field and short-range forces of the MM model at the boundaries of the QM cluster. At the onset of a calculation when the QM cluster is a fragment of a regular surface, the sites of the environment should be located at the MM equilibrium positions. For this purpose, the QM/MM interface is constructed so that forces at the cluster boundary are balanced with respect to the regular MM fragment [3, 6]. In general, any structural changes in the active site result in the relaxation of the QM cluster and its MM environment. Concerted embedding in the EPE method makes it possible to perform the full optimization of an isolated defect with consideration for cluster environment polarization even for complicated cases such as the reconstruction of polar surfaces [7].

In the case of the separation of the QM cluster from the lattice of a covalent crystal, its boundary atoms have artificially formed bonds. The adaptation of the EPE method to describe oxides with polar covalent bonds (covEPE) [8, 9] includes specially constructed monovalent pseudo-oxygen centers (O*) arranged at the oxygen positions of a real lattice but forming only a single bond with the QM cluster similarly to the fluorine atom. To avoid the artificial polarization of anionic O* sites by the nearest point charges of the environment, these Si sites are simulated as cationic effective potentials $Si^{PP}$* with the same effective charge as in their MM analogs, as in the above EPE scheme for ionic oxides. The corresponding mutual polarization of the QM cluster and ions in its environment was provided by choosing the point charges of MM sites so that the electrostatic potential (ESP) of the corresponding MM crystal fragment reproduced the ESP of an analogous QM fragment. For this purpose, a special force field was developed with the use of a shell model based on the ESP charges of 1.2 a.u. for Si and –0.6 a.u. for atoms [9].

## METAL PARTICLES ON OXIDE SUBSTRATES AND IN ZEOLITES

### *Single d-Metal Atoms on the MgO(001) Surface*

The MgO(001) surface is a simple model example of a stable nonpolar (stoichiometric) surface with pronounced basic properties. The ability of this surface to immobilize metal atoms and clusters is due to the properties of low-coordinated oxygen atoms and oxygen vacancies—$F_s$ and $F_s^+$ centers.

We studied the structure and properties of chemical bonds in adsorption complexes formed by 17 different single transition metal atoms (Cr, Mo, W, Mn, Re, Fe, Ru, Os, Co, Rh, Ir, Ni, Pd, Pt, Cu, Ag, and Au) upon adsorption at the anions of the regular MgO(001) surface and corresponding $F_s$ and $F_s^+$ point defects by quantum-chemical calculations [10, 11] with the use of an all-electron scalar-relativistic density functional method (gradient-corrected functionals BP86 and PBEN) and EPE schemes for a cluster embedded in the lattice of ionic materials. Figure 1 shows characteristic variations in the calculated binding energies in the given adsorption complexes.

Within a group of the periodic table, 3*d* atoms, in general, were found to adsorb at the $O^{2-}$ site more strongly than 4*d* atoms, but more weakly than 5*d* atoms. With few exceptions, *d*-metal atoms interact with anions at the regular surface much more weakly that with oxygen vacancies. In this case, electron-density transfer to the adsorbate was considerable in the adsorption complexes of these metals. Considering binding energy changes over a period, we observed a small destabilization of Group VII complexes with reference to their Group VI analogs. Next, an increase in binding energies up to Group XI was observed in each period. On going to Group XI, the binding energy decreased moderately for $O^{2-}$ and $F_s^+$ vacancies or considerably for $F_s$ vacancies. In general, changes in

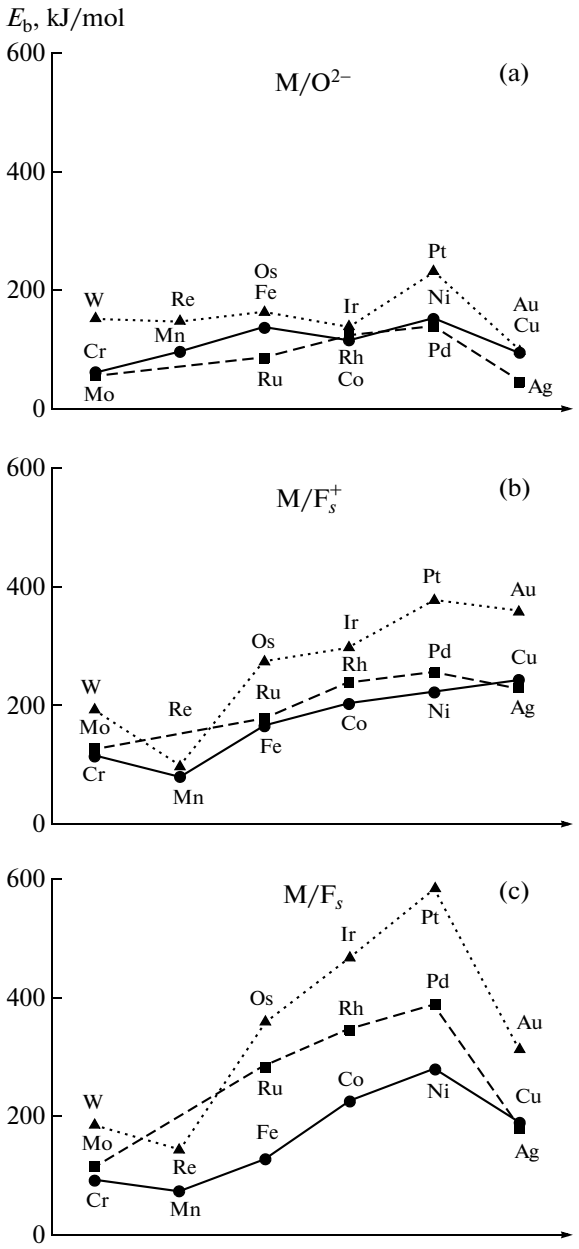


**Fig. 1.** Calculated binding energies ($E_b$) of single transition metal atoms (Cr, Mo, W, Mn, Re, Fe, Ru, Os, Co, Rh, Ir, Ni, Pd, Pt, Cu, Ag, and Au) with (a) oxygen sites on the ideal MgO(001) surface and with (b) $F_s^+$ and (c) $F_s$ oxygen vacancies on the defect MgO(001) surface.

binding energies correlated with changes in the effective charges of adsorbates and corresponding changes in the electrostatic interaction of the adsorbate with the active site of the substrate. Thus, the binding energy of a metal on the substrate in $M/F_s^+$ complexes was noticeably lower than energies in their $M/F_s$ analogs. This difference is determined by a greater electrostatic stabilization of neutral complexes, in which electron density accumulation at *d*-metal atoms is more significant. As in the case of Cu, Ag, and Au atoms, $M/F_s^+$ complexes rather than $M/F_s$ complexes can be energetically more favorable with the predominance of covalent interactions. All of the test complexes did not exhibit signs of the oxidation of *d*-metal atoms.

Our calculations suggest the dependence of the shifts of core levels in *d*-metal atoms adsorbed on MgO(001) on the type of adsorption complexes. Based on the calculated adsorption energies and core level energies, we can predict experimental results for metal atoms adsorbed at the terraces of the MgO(001) surface. These data are mainly consistent with the results of an XPS study performed by Lee et al. [12] for $Au/TiO_2(110)$. Thus, for example, the data obtained for Au, Ag, and Cu atoms suggest that the surface diffusion of Ag atoms followed by immobilization at oxygen vacancies will occur at lower temperatures than that in the case of Cu and Au because Ag interacts with $O^{2-}$ more weakly than Cu or Au. Diffusion, which results in the formation of $M/F_s$ complexes, will result in a moderate positive shift of 0.4–0.6 eV in metal core levels. On the other hand, the formation of $M/F_s^+$ complexes will be accompanied by negative shifts, as compared with $M/O^{2-}$ complexes.

### *Single d-Metal Atoms on the Polar α-$Al_2O_3$(0001) Surface*

Unlike the nonpolar MgO(001) surface, clear polar surfaces are usually inadequately stable to occur in a defect-free unreconstructed and nonhydroxylated form [13]. The $\alpha$-$Al_2O_3$(0001) surface the top layer of which is formed by aluminum cations is an example of these surfaces. It has been actively studied as the prototype of a surface with the strong relaxation of its initial geometry to decrease the effect of charge separation [14]. The adsorption of individual Pd [15], Pt [15], and Au [16] atoms at the surface sites of $\alpha$-$Al_2O_3$(0001) was also studied using the EPE model.

As well as *d*-metal atoms on MgO(001), Pd, Pt, and Au atoms adsorb on the $\alpha$-$Al_2O_3$(0001) surface at $O^{2-}$ sites. The adsorption energies of Pd, Pt, and Au (110, 165, and 45 kJ/mol, respectively) are 21–57 kJ/mol smaller than the corresponding energies of adsorption on MgO(001). Unlike the adsorption on MgO(001), the metal atom adsorbed at the oxygen site of the $\alpha$-$Al_2O_3$(0001) surface simultaneously interacts with a neighboring cation from the top layer of the surface. The ionic component of the chemical bond of the most stable adsorption complexes on $\alpha$-$Al_2O_3$(0001) is very small because the effective charges of adsorbed atoms are small: 0.2 a.u. for Pd, 0.3 a.u. for Pt, or even a small negative charge (–0.14 a.u.) for Au. The binding energies of metal atoms in other possible adsorption positions over the centers of equilateral oxygen

triangles were at least 40 (Pd) or 125 (Pt) kJ/mol smaller than that for adsorption at $O^{2-}$ sites. These structures do not correspond to local minimums in an energy hypersurface, and they characterize surface diffusion barriers.

### *Oligomeric Complexes of Gold Subgroup Metals on the MgO(001) Surface*

We studied the adsorption of small clusters $M_n$ (M = Cu, Ag, and Au; $n = 2$ or 3) at $O^{2-}$ sites and Cu, Ag, and Au dimers at the $F_s$- and $F_s^+$ sites of the MgO(001) surface [17]. Upon adsorption on the regular MgO(001) surface, the $M_2$ cluster is arranged perpendicularly to the surface over $O^{2-}$ anions, as well as adsorbed single atoms. The most stable complex structures with a dimer axis parallel to the surface are at least 20 kJ/mol less stable. The calculated binding energies of the most stable structures are 96 ($Cu_2$), 32 ($Ag_2$), and 132 kJ/mol ($Au_2$).

On the regular MgO(001) surface, $Cu_3$ clusters most strongly adsorb perpendicularly to the surface with two atoms of the $M_3$ triangle coordinated to two neighboring oxygen atoms (surface complex A). The adsorption energy of this cluster is 192 kJ/mol. We also identified two other adsorption complexes with close binding energies of 159 (B) and 153 kJ/mol (C). Complex B differs from complex A in that the plane of the $M_3$ triangle is inclined to the oxide surface. The $Cu_3$ triangle has a short and two long sides, and it is structurally similar to the geometry of the free $Cu_3$ cluster having the electron configuration $2A^1$. In the structure of C, only one of the Cu atoms is coordinated to a surface anion and the $Cu_3$ triangle is nearly equilateral. For $Ag_3$ and $Au_3$, complex A is also most stable with adsorption energies of 106 and 192 kJ/mol, respectively. Complexes C are characterized by adsorption energies of 90 ($Ag_3$) and 168 kJ/mol ($Au_3$), which are close to those of complexes A. At the same time, complexes B for $Ag_3$ and $Au_3$ clusters are two times more weakly bound to the surface than complexes A.

Comparing the binding energies of single M atoms with the MgO(001) surface and the binding energies per atom in free $M_2$ and $M_3$ clusters, we can see that bonds with the surface compete to an extent with intracluster bonds. The adsorption energy of silver atoms (46 kJ/mol) was found especially low; it is about a half of the specific dissociation energy ($D_e/n$) of a dimer or trimer (81 kJ/mol per atom). This energy ratio is consistent with the lowest adsorption energies for silver dimers and trimers, as compared with their analogs for copper and gold.

We considered three orientations of gold subgroup metal tetramers adsorbed on MgO(001): two structures with an orientation of $M_4$ perpendicular to the surface, in which the $M_4$ rhombus is coordinated to the surface through two (complex A) or one (complex B) atoms, and a structure with an orientation of $M_4$ parallel to the surface (complex C) [18]. Adsorption insignificantly distorted the gas-phase rhombus-planar structure. Complexes A were found most stable with adsorption energies of 191 (Cu), 112 (Ag), and 216 kJ/mol (Au). The adsorption energies of complexes with the orientation of the $M_4$ cluster parallel to the surface were lower by a factor of more than 2. Unlike A, complexes B and C are local minimums only in calculations performed in the $C_{2v}$ symmetry.

The chemical bond between an $M_2$ dimer and an $F_s$ vacancy can be described by the interaction of a doubly filled orbital of the vacancy and the $\sigma^*$ lowest unoccupied molecular orbital (LUMO) of $M_2$. The interaction energies of dimers with $F_s$ sites were found higher than the corresponding interaction energies with $O^{2-}$ oxygen sites by a factor of 1.6–2.7, and they correlated well with the LUMO orbital energy of $M_2$ dimers. In the case of $Cu_2$ and $Ag_2$ dimers, LUMOs are located somewhat lower than the occupied orbital of the vacancy, whereas the LUMO of $Au_2$ is lower than the vacancy level by approximately 2 eV. Therefore, the electron affinity of the gold dimer is higher than the electron affinities of copper and silver dimers. Correspondingly, $Cu_2$ and $Ag_2$ exhibited similar adsorption energies of about 214 kJ/mol, and $Au_2$ adsorbed with a much higher energy of 392 kJ/mol. Considerable electron-density transfer was observed in $Cu_2/F_s$, $Ag_2/F_s$, and $Au_2/F_s$ complexes. The effective charges of the adsorbed dimers are –0.80, –0.83, and –0.73 a.u., respectively. Adsorption at $F_s^+$ charged oxygen vacancies is described by the same orbital interaction as for $F_s$; however, the interaction energies with $F_s^+$ sites are as low as ~60% of the corresponding energies of complexes with $F_s$ sites because, unlike a neutral vacancy, the orbital of a charged defect is occupied by only a singe electron. In this connection, the effective charges of dimers adsorbed at $F_s^+$ are approximately a half of dimer charges at $F_s$ sites.

We also studied the $Cu_4$, $Ag_4$, and $Au_4$ clusters adsorbed at the $F_s$ and $F_s^+$ oxygen vacancies of MgO(001) [19]. In the most stable configuration, the $M_4$ rhombus is adsorbed perpendicularly to the MgO(001) surface. In this case, a metal atom is coordinated to an oxygen vacancy and another atom forms a bond with the oxygen atom closest to the vacancy. The adsorption energies at $F_s$ and $F_s^+$ sites are 305 and 220 ($Cu_4$), 284 and 159 ($Ag_4$), and 475 and 327 kJ/mol ($Au_4$), respectively. This strong interaction, as compared with that in dimers and trimers, with oxygen vacancies and, especially, $F_s$ sites can be explained to a considerable extent by a large effective negative charge of $M_4$. As in the case of $M_2$ and $M_3$ complexes, $Au_4$ is most strongly adsorbed; the next are $Cu_4$ and $Ag_4$ clusters in terms of bond strength.

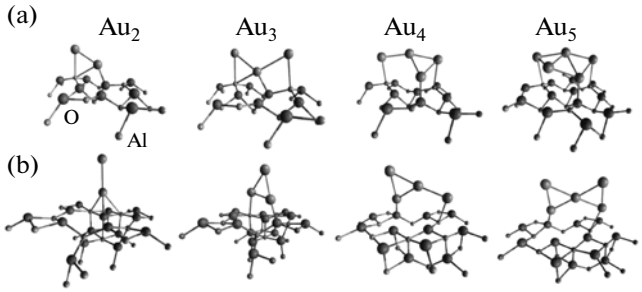


**Fig. 2.** Equilibrium structures of the adsorption complexes formed by $Au_n$ particles ($n$ = 1–5) on the (a) α-$Al_2O_3$(0001) and (b) γ-$Al_2O_3$(001) surfaces.

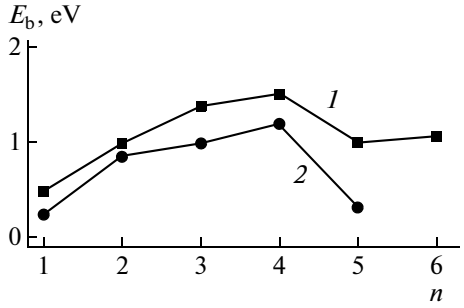


**Fig. 3.** Adsorption energies of $Au_n$ on the (*1*) α-$Al_2O_3$(0001) and (*2*) γ-$Al_2O_3$(001) surfaces.

### *$Pd_3$ and $Pt_3$ Clusters on the α-$Al_2O_3$(0001) Surface*

Nasluzov et al. [20] studied the cluster models of $Pd_3$ and $Pt_3$ adsorption complexes on the Al-terminated α-$Al_2O_3$(0001) surface. In its topology, the α-$Al_2O_3$(0001) surface is suitable for the formation of an interface with hexagonal metal surfaces, in which each surface anion interacts with an atom from a metal layer. It is well known that thin alumina films facilitate the growth of supported metal nanoclusters having an interface of a similar type [21]. The $M_3$ clusters adsorbed collaterally to the surface are the simplest example of this kind, in which the number of contacts between the supported metal and surface oxygens reaches a maximum. At the same time, in the complexes thus formed, the surface anions ($O^{2-}$) occupy ligand positions that are nonoptimal for $M_3$. As an alternative, the $M_3$ adsorption complexes with an orientation perpendicular to the surface seem energetically preferable. The predominant formation of particular structures depends on the abilities of the support and the adsorbate to undergo structural rearrangements to optimize contacts for strong coordination interaction. In the case of $Pd_3$ and $Pt_3$ trimers, complexes with an orientation perpendicular to the surface are more stable, as in the case of gold subgroup metal clusters. The structural characteristics of the resulting complexes are similar, although the adsorption energies differ considerably: 210–250 and 105–145 kJ/mol for $Pt_3$ and $Pd_3$, respectively. In these structures, an atom at the base of the $M_3$ triangle is attached to a surface anion, whereas the other M atom interacts with two neighboring surface anions. Because of this type of adsorption, the structure of the α-$Al_2O_3$(0001) surface is strongly distorted near the adsorbed $M_3$ cluster so that the $M_3$ nearest-neighbor cations in the top surface layer are elevated by 30–40 pm.

### *Small Gold Clusters $Au_n$ on α-$Al_2O_3$(0001) and γ-$Al_2O_3$(001)*

To compare the chemical bonds of gold clusters on various modifications of hydroxylated alumina surfaces, we calculated small gold clusters $Au_n$ on α-$Al_2O_3$(0001) ($n$ = 1–6) and γ-$Al_2O_3$(001) ($n$ = 1–5) [16]. In a gas phase, these small gold clusters are characterized by a planar structure [22, 23]. As other clusters [24, 25], the small gold clusters also considerably retained their structure peculiarities in the case of their adsorption (Fig. 2). In the test adsorption complexes, the adsorbate and the support interact with the formation of Au–O bonds (207–211 pm) and additional Au–Al contacts (248–273 pm). On α-$Al_2O_3$(0001), gold clusters form a band with a surface anion and to three bonds with cationic surface sites. The number of cationic contacts increases with cluster size; in the case of great values of $n$, it can be seen that the adsorbed gold cluster is a nucleus of a monatomic layer that begins to cover the surface. On γ-$Al_2O_3$(001), small gold clusters adsorb with an orientation perpendicular to the (001) surface. The $Au_n$ clusters interact with a surface anion, whereas the clusters with $n$ = 3–5 additionally interact with a cationic site. As compared with α-$Al_2O_3$(0001), the Au–Al bond lengths in complexes on γ-$Al_2O_3$(001) are greater (266–280 pm). On the contrary, the Au–O bonds with low coordinated surface anions on γ-$Al_2O_3$(001) are shorter (204–208 pm) and, probably, stronger. The calculated Au–O bond lengths for both surface types are consistent with EXAFS spectroscopic data for gold clusters on the polycrystalline samples of aluminum oxide; according to these data, the Al–O bond lengths fall within the range of 204–210 pm [9].

The binding energy ($E_b$) for each alumina surface type increases with gold cluster size ($n$) up to tetramers (Fig. 3). However, an increase in the energy was not observed on going to $Au_5$ or $Au_6$ clusters. On the α-$Al_2O_3$(0001) surface, gold clusters adsorb with high binding energies of 43–147 kJ/mol. In large clusters, noticeable negative contributions to the energy of adsorption due to a noticeable distortion of their planar structure appeared. On the γ-$Al_2O_3$(001) surface, the planar structure was also retained for gold clusters adsorbed perpendicularly to the surface. The binding energies on γ-$Al_2O_3$(001) were somewhat lower than those of the corresponding complexes on α-$Al_2O_3$(0001) (24–114 kJ/mol). Small gold clusters interact with alumina surfaces more weakly than with

the strongly basic MgO(001) surface, where the binding energies fall within the range of 94–216 kJ/mol [17]. However, the adsorption energies of $Au_n$ on MgO(001) also increase with cluster size to $n = 4$. On the contrary, the adsorption energy of the $Au_6$ cluster on the $\alpha$-$Al_2O_3$(0001) surface (100 kJ/mol) is higher than that of the $Au_6$ cluster immobilized on zeolite (~83 kJ/mol) [26].

Adsorbed $Au_n$ particles on various alumina surfaces have negative effective charges from –0.09 to –0.14 a.u. on $\alpha$-$Al_2O_3$(0001) and from –0.17 to –0.30 a.u. on $\gamma$-$Al_2O_3$(001). The atoms of polynuclear adsorption complexes that directly interact with oxygen atoms are positively charged (0.07–0.31 a.u.). Other atoms of the complex are characterized by small, primarily negative, effective charges (–0.26–0.09 a.u.). The comparatively small absolute values of charges suggest that the adsorbed gold clusters bound to low coordinated surface ions do not undergo oxidation or reduction. As noted previously, the interaction of metal clusters with an oxide substrate in the case of aluminum and magnesium oxides is mainly due to adsorbate polarization in an electrostatic field of the surface and the Pauli repulsion between the occupied orbitals of the substrate and adsorbate.

### *Gold Atoms and Dimers on the Surface of Amorphous $SiO_2$*

The optical properties of gold atoms and dimers adsorbed on the surface of amorphous $SiO_2$ were studied both experimentally and theoretically [27, 28]. The experimental spectra were recorded using cavity ringdown spectroscopy [29, 30]. For the correct attribution of these spectra, DF calculations were performed in a free cluster approximation and with the use of a periodic supercell [28, 31]. The main electron transitions of adsorbed gold atoms and dimers were calculated using the time-dependent DF method. The experimental spectra of adsorbed gold atoms were characterized by three bands at 1.95, 2.48, and 2.75 eV, whereas the gold dimer had four bands at 1.90, 2.15, 2.35, and 2.58 eV.

Various defects on the surface of $SiO_2$ were considered. Among them, only silicon dangling bonds (≡Si$^\bullet$), nonbridging oxygen (≡Si–O$^\bullet$) centers, and silanolate groups (≡Si–O$^-$) served as adsorption sites for gold particles. The main calculated electron transition in the ≡Si–Au surface complex (4.02 eV) is beyond the experimentally detected range. At the same time, electron transitions for the ≡Si–O–Au complex fall within this range. The calculated transitions at 2.59 and 2.20 eV were ascribed to the main experimental band at 2.48 eV and a weak band at 1.95 eV, respectively. The electron transitions calculated for the ≡Si–O–Au$^-$ complex well reproduced the experimental spectrum. Transitions at 2.07 and 2.14 eV were ascribed to an experimental band at 1.95 eV, whereas a transition at 2.86 eV was close to an experimental band at 2.75 eV. Thus, the spectrum of $Au_1/SiO_2$ can be completely attributed assuming the simultaneous occurrence of ≡Si–O$^\bullet$ and ≡Si–O$^-$ groups on the surface. In the case of the ≡Si–O–$Au_2$ complex, only transitions at 2.35 and 2.66 eV fall within the range of the experimentally recorded spectrum, and they can be ascribed to bands at 2.35 and 2.58 eV, respectively. A weak experimental band at 2.15 eV can be due to the transition at 2.17 eV, which was calculated for the ≡Si–$Au_2$ complex. All of the other transitions calculated for this complex, as well as all of the transitions for ≡Si–O–$Au_2^-$ groups, lie above the experimental range. Consequently, the spectrum of $Au_2/SiO_2$ depends on transitions in ≡Si–O–$Au_2$ and, probably, ≡Si–$Au_2$ complexes.

### *Metal Particles in Zeolite Cavities*

The adsorption of metal particles on the surfaces of covalent oxides, such as microporous silicates or aluminosilicates (zeolites), is of special chemical interest. The three-dimensional structure of zeolites with a system of narrow channels allows them to sorb only nanosized particles on their inner surfaces. Moreover, interactions with the active sites of a zeolite substrate can change the structure and properties of small metal particles. Thus, adsorption at acidic hydroxyl groups with labile protons can cause proton migration from the substrate to metal particles [32]. Indeed, calculations performed using simple cluster models demonstrated [33, 34] that $M_6$ clusters (M is an element from Groups VIII–XI of the periodic table) adsorbed at OH groups mainly occur as $M_6H_3$ hydrides rather than free $M_6$ clusters. However, because the energy effect of the formation of hydride species for metal clusters (for example, $Ag_6$ and $Au_6$) is very small, these results of model studies cannot be considered as ultimate.

Proton transfer from zeolite OH groups to metal clusters (this process is also referred to as reversible proton spillover) was studied using a version of the covEPE embedding scheme adapted to systems with polar covalent bonds [8, 9]. This scheme takes into account two important aspects, which were ignored in simple cluster models: the elasticity of a zeolite latter and the electrostatic effects of a zeolite environment. A faujasite substrate was represented by a model of QM cluster 12T containing 12 centers in the tetrahedral (T) positions of the zeolite. The central six-membered ring of this model was a part of sodalite cell directed to the faujasite supercavity. Three zeolite OH groups were localized in different crystallographic positions, and the simultaneous transfer of all of the three protons was considered [26]. The covEPE calculations demonstrated that a correct consideration of the effects of a zeolite environment decreased the energy effect of proton transfer to metal clusters by 50–70 kJ/mol (on a proton basis), as compared with calculations on finite substrate models. The reversible

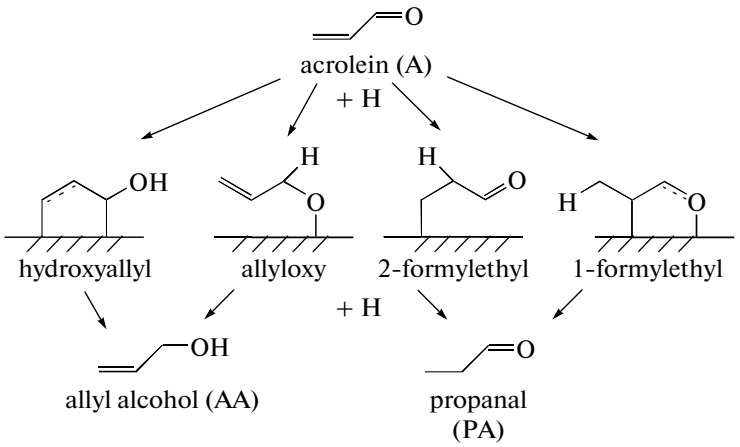


**Fig. 4.** Elementary steps of the reaction of partial acrolein hydrogenation on the surface of silver catalysts.

hydrogen spillover remained much more favorable for $Rh_6$ (by 73–98 kJ/mol per proton) and $Ir_6$ clusters (by 144–160 kJ/mol per proton). The energy effect of spillover to the $Au_6$ cluster changed depending on the positions of OH groups, that is, on their acidity. Proton migration from less acidic OH groups in O4 crystallographic positions was endothermic (29 kJ/mol), whereas transfer from more acidic OH groups in O3 positions was exothermic (47 kJ/mol). Thus, the covEPE study allowed us to detect the first example when the defect-free form of the $M_6$/zeo(3H) cluster is energetically more favorable than the hydrogenated form $M_6$(3H)/zeo. The decrease in proton spillover energies can be explained using a more realistic zeolite model. The $M_6$ particles weakly interacting with the substrate underwent more pronounced structural changes in the covEPE model; consequently, they were stabilized more strongly than their hydride analogs ($M_6H_3$), which were more strongly bound to a dehydroxylated oxygen sites, and, correspondingly, they were less dependent on the procedure used for simulating the zeolite environment.

## REACTIONS ON METAL PARTICLES AND METAL SURFACES

### *Mechanism of the Selective Hydrogenation of α,β-Unsaturated Aldehydes on Silver Catalysts*

The partial hydrogenation of α,β-unsaturated aldehydes to unsaturated alcohols is of commercial importance as a source of reagents for the manufacture of pharmaceuticals, perfumery, and food flavors [35, 36]. Unlike platinum group metals [35, 36], supported silver catalysts [37] exhibited relatively high selectivity (~50%) in the hydrogenation of acrolein to allyl alcohol (Fig. 4) [38]. Note that the formation of a competing product (the saturated aldehyde propanal) is thermodynamically more favorable. It was found that reaction conditions considerably affected the characteristics of the catalyst [39]. In particular, recently, Bron et al. [40] demonstrated a positive effect of oxygen pretreatment on the activity and selectivity of the $Ag/SiO_2$ catalyst in the partial hydrogenation of acrolein. Nevertheless, the reaction mechanism remains unclear on the molecular level: the activity of silver as a hydrogenation catalyst is surprising because it is well known that the ability of pure silver single-crystal surfaces to activate $H_2$ molecules is low [41].

**Hydrogen activation on an oxidized surface of Ag.** Recently, we considered in detail the activation of $H_2$ on various Ag surfaces with the use of DF calculations [41, 42]. According to the calculations, the dissociation of $H_2$ on low-index silver surfaces is thermodynamically and kinetically unfavorable (the endothermic effect is ~40 kJ/mol, and activation barriers are ~125 kJ/mol) [41]. The passivity of Ag in hydrogen activation is dramatically different from the properties of platinum group metals, on which molecular hydrogen undergoes almost barrierless dissociation [43]. Thus, to explain the ability of Ag to catalyze hydrogenation reactions, the possibility of surface modification in the course of catalytic reaction or as a result of catalyst pretreatment should be considered. To reveal the potential sources of atomic hydrogen, which acts as a reactant in the hydrogenation of organic molecules on silver catalysts, we calculated the dissociation of $H_2$ on various model oxygen sites arranged both on the surface of Ag and in a subsurface region: O/Ag(110), OH/Ag(110), $p(2 \times 1)$O/Ag(110), $p(2 \times 1)$OH/Ag(110), and $O_{sub}$/Ag(111) [41, 42]. It was found that all of the above oxygen sites facilitate the dissociation of $H_2$ [41, 42]. An analogous effect was obtained in another computational work for the partially oxidized surface of Ag [44]. These results imply that a noticeable increase in activity in the course of hydrogenation, which was observed after the oxygen pretreatment of catalysts based on supported Ag [40], can be a consequence of a higher rate of $H_2$ dissociation with the formation of adsorbed H atoms on the partially oxidized regions of the surface of Ag.

**Reaction paths of acrolein hydrogenation on the Ag(111) and $O_{sub}$/Ag(111) surfaces.** The structure of the experimentally studied hydrogenation catalysts based on supported Ag particles is complicated; their properties are considerably changed under reaction conditions, and reliable data on the nature of active sites are currently unavailable [39]. Thus, to improve the understanding of the catalytic effect of a silver component, we performed simulation for two limiting cases: a clean extended surface and an extended surface modified with subsurface oxygen ($O_{sub}$), which are referred to as Ag(110) and $O_{sub}$/Ag(111), respectively [45]. The competing reaction paths (Fig. 4) leading to allyl alcohol or propanal were studied with the localization of transition states and the calculation of activation barriers for a considerable number of the elementary steps of hydrogenation.

According to the results of DFT calculations [45], undesirable propanal is the main product on the Ag(110) surface. This is consistent with the low selectivity for allyl alcohol (~10%) observed in the hydrogenation of acrolein on bulk silver catalysts [39]. As a consequence of the weak adsorption of acrolein on the surface of silver [46], no indications of the predominant activation of the C=O bond, as compared with C=C [45], were detected, whereas this bond activation is usually assumed as a necessary prerequisite for the selective hydrogenation of the carbonyl group [35, 36]. The $O_{sub}$/Ag(111) model system exhibited a lower activity in the hydrogenation of acrolein by adsorbed H atoms, as compared with a clean surface of Ag [45]. However, for the reaction on the $O_{sub}$/Ag(111) surface, the calculated selectivity for allyl alcohol was extremely high [45], and this result can be compared with the experimentally observed increase in catalyst selectivity after oxidative treatment [40]. On the Pt(111) surface [47, 48], low selectivity for allyl alcohol was explained by the hindered desorption of this product, which finally resulted in its complete hydrogenation into a saturated alcohol. On the contrary, in the Ag(110) and $O_{sub}$/Ag(111) model silver systems, calculations predicted the rapid desorption of both of the products (allyl alcohol and propanal) under the standard conditions of hydrogenation reaction [45].

According to DF calculations, the mechanism of action of Ag-based catalysts [41, 42, 45, 46] in the reaction of acrolein hydrogenation differs from the mechanism of action of Pt-based catalysts in many characteristics [47, 48]. This result seems conceptually important for the development of efficient catalysts for the selective hydrogenation of organic substances having multiple unsaturated functional groups. Of course, experimental and theoretical studies should be continued for the more comprehensive explanation on a microscopic level of all of the unusual properties of silver as a catalyst for hydrogenation processes. It would be especially desirable to detect and identify the nature of active sites involved in the formation of atomic hydrogen and to study the activity of various defects in the structure of these catalysts.

### *C–O Bond Cleavage in the Course of Methanol Decomposition on Pd Nanocrystallites*

The manufacture of hydrogen from methanol is directly related to a practically important problem of the development of transport facilities with the use of methanol as a fuel [49]. The decomposition of $CH_3OH$ on catalysts based on Pd with high selectivity yields CO and $H_2$ [50, 51]. However, in general, the activity of the system is limited because of the gradual accumulation of $CH_x$ ($x = 0–3$) formed as the by-products of methanol decomposition on the surface of particles [52–54]. It is believed that the $CH_x$ carbon residues result from the cleavage of C–O bonds either in methanol or in the $CH_xO$ intermediates of methanol dehydrogenation [52, 55]. However, it remains unclear in which particular intermediates and at which step of dehydrogenation C–O bond cleavage is most probable.

The reaction paths of C–O bond cleavage in various intermediates formed in the decomposition of methanol on Pd nanoparticles were studied with the use of the DF method [56]. Because, as a rule, the active component of catalysts has a complex morphology, three-dimensional clusters seem more realistic models than ideal surfaces with periodic boundary conditions for a theoretical study of catalytic systems. Invoking our recently proposed modeling strategy that relies on nanoclusters bounded by small-index crystal planes [57–60], a $Pd_{79}$ truncated octahedral nanocluster was chosen as a model of highly ordered supported metal particles containing about $10^3$–$10^4$ Pd atoms [52–54]. This model approach makes it possible to study the effects of various structural inhomogeneities, such as particle edges [57, 58], on the catalytic properties of metal nanoparticles as well as size effects [60]. The total symmetry of models based on a $Pd_{79}$ truncated octahedron (Fig. 5) was reduced to a sufficient degree in order to remove local limitations on the structure of an adsorption complex on the nanocluster surface. Thus, the adsorption characteristics of various methanol decomposition intermediates ($CH_3OH$, $CH_3O$, $CH_2OH$, $CH_2O$, CHO, and CO) and transition states corresponding to C–O bond cleavage in these intermediates were studied [59].

The C–O bond dissociation energies calculated for the above intermediates and the corresponding activation barriers suggest that the cleavage of the C–O bond can occur as an extremely slow side process, whereas the main reaction path is methanol dehydrogenation with the formation of CO and hydrogen. In the side process, the cleavage of ordinary ($\sigma$-type) C–O bonds in $CH_3O$ and $CH_2OH$ intermediates is most probable [56]. The presence of a $\pi$ contribution (as in $CH_2O$ and CHO intermediates) results in a considerable increase in the activation barrier of C–O bond cleav-

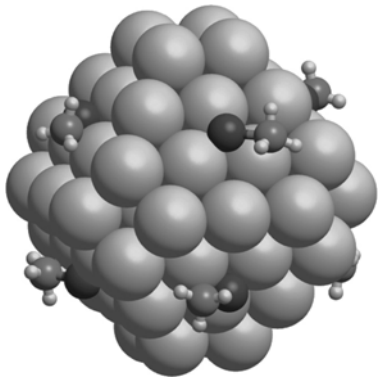

**Fig. 5.** Truncated octahedron of $Pd_{79}$ with adsorbates arranged at (111) faces within $D_4$ symmetry. As an example, the transition state of methoxide dissociation into O and $CH_3$ fragments is shown.

age. The highest activation barriers were calculated for the dissociation of the adsorbed molecule of CO, the end product in the process of methanol decomposition. This is no wonder because the bond in this molecule is strongest due to a considerable $\pi$ contribution. Moreover, according to calculated data, the dissociation of CO on a Pd nanoparticle is strongly endothermic [56]. These results are consistent with experimental observations suggesting that the dissociation of CO molecules does not occur even upon adsorption on a highly defect surface of Pd [53].

Previously, it was hypothesized that the C–O bond was primarily cleaved in intermediates with the axis of this bond declined from a normal to the surface; consequently, the bond can be considered more activated because of adsorption interaction [55]. According to this model, the molecules of formaldehyde ($H_2CO$) and formyl (HCO) seemed the most probable candidates for performing this process. In the adsorption complexes of these molecules, the C–O axis is almost parallel to the surface of Pd, whereas the C–O axis in adsorbed methoxide ($H_3CO$) or the CO molecule is perpendicular to the surface [53]. However, from the results of the calculations of activation barriers [56], it follows that the orientation of the C–O bond with respect to the surface of Pd is a secondary factor in the bond cleavage mechanism in the decomposition of methanol.

According to experimental observations, the accumulation of $CH_x$ carbon residues ($x = 0–3$) upon methanol degradation on Pd nanocrystallites primarily occurs near edges between (111) faces and other defects [53]. The role of low coordinated (edge) positions in the poisoning of the surface of a catalytic Pd particle by $CH_x$ fragments was also studied theoretically [56]. In particular, the results of calculations indicate that the $CH_3$ and $CH_2$ species formed upon the degradation of $CH_3O$ and $CH_2OH$ are stabilized at the edges of the $Pd_{79}$ cluster. In this case, the dehydrogenation of the $CH_3$ and $CH_2$ species to CH and C, which form the strongest adsorption bonds with the surface, can rapidly occur.

Carbon residues on the surface of palladium catalysts resulting from the slow decomposition of various simple organic reagents have attracted considerable attention in recent years because it was found that the presence of these residues increases the selectivity of alkyne hydrogenation to alkenes [61–64]. It is believed that carbon atoms occupying interstitial positions in the nearest subsurface region of Pd play a crucial role in increasing selectivity; thus, they prevent the participation of hydrogen dissolved in the bulk in the hydrogenation reaction, which occurs on the surface [61–64]. Indeed, the DF calculations demonstrated that the adsorbed monatomic carbon species can penetrate into subsurface interstitial positions [65]. This process is exothermic, and it is characterized by a relatively low activation barrier [66]. Recently, it was calculated that the migration of C atoms on Pd nanoparticles into a subsurface region occurs near cluster edges with smaller energies than at regular faces [67]. Nevertheless, as calculated with the use of Pd(111) as an example, the formation of polyatomic $C_2$ and $C_3$ species, which are the precursors of the most stable graphene-like phase, at higher surface coverages with carbon (~0.5 of a monolayer) begins to compete with the diffusion of C monomers into the subsurface region [68].

## ACKNOWLEDGMENTS

We are grateful to K.M. Neyman and G.N. Vayssilov for their great role in the long-term cooperation in this field of research. We are also grateful to U. Birkenheuer, A.B. Gordienko, C. Inntam, R.N. Kosarev, S.M. Kozlov, K.H. Lim, A.V. Matveev, A.B. Mohammad, L.V. Moskaleva, G. Pacchioni, V.V. Rivanenkov, and O.Z. Zakharieva for their contributions to this work.

This study was supported by the Deutsche Forschungsgemeinschaft, the Volkswagen Foundation, INTAS, the Russian Foundation for Basic Research (project no. 10-03-00441), the Siberian Branch of the Russian Academy of Sciences (integration project nos. 26 and 79), the Russian Science Support Foundation, and the Fonds der Chemischen Industrie (Germany).

## REFERENCES

1. Pacchioni, G., Bagus, P.S., and Parmigiani, F., *Cluster Models for Surface and Bulk Phenomena*, NATO ASI Series B, New York: Plenum, 1992, vol. 283.
2. Belling, T., Grauschopf, T., Krüger, S., Nörtemann, F., Staufer, M., Mayer, M., Nasluzov, V.A., Birkenheuer, U., Hu, A., Matveev, A.V., Shor, A.M., Fuchs-Rohr, M.S.K., Neyman, K.M., Ganyushin, D.I., Kerdcharoen, T., Woiterski, A., Gordienko, A.B., Majumder, S., and Rösch, N., *ParaGauss Version 3.0*, Munich: Technische Universität München, 2004.

3. Nasluzov, V.A., Rivanenkov, V.V., Gordienko, A.B., Neyman, K.M., Birkenheuer, U., and Rösch, N., *J. Chem. Phys.*, 2001, vol. 115, p. 8157.
4. Catlow, C.R.A. and Markrodt, W.C., in *Computer Simulation of Solids. Lecture Notes in Physics*, Catlow, C.R.A. and Markrodt, W.C., Eds., Berlin: Springer, 1982, vol. 166, p. 3.
5. Lidiard, A.B., *J. Chem. Soc., Faraday Trans. 2*, 1989, vol. 85, p. 341.
6. Nasluzov, V.A., Rivanenkov, V.V., Shor, A.M., Neyman, K.M., Birkenheuer, U., and Rösch, N., *Int. J. Quantum Chem.*, 2002, vol. 90, p. 386.
7. Noguera, C., Pojani, A., Finocchi, F., and Goniakowski, J., *Chemisorption and Reactivity on Supported Clusters and Thin Films: Towards an Understanding of Microscopic Processes in Catalysis*, NATO ASI Series E, Dordrecht: Kluwer, 1997, vol. 331, p. 455.
8. Nasluzov, V.A., Ivanova, E.A., Shor, A.M., Vayssilov, G.N., Birkenheuer, U., and Rösch, N., *J. Phys. Chem. B*, 2003, vol. 107, p. 2228.
9. Shor, A.M., Ivanova-Shor, E.A., Nasluzov, V.A., Vayssilov, G.N., and Rösch, N., *J. Chem. Theory Comput.*, 2007, vol. 3, p. 2290.
10. Neyman, K.M., Inntam, C., Nasluzov, V.A., Kosarev, R., and Rösch, N., *Appl. Phys. A*, 2004, vol. 78, p. 823.
11. Neyman, K.M., Inntam, C., Matveev, A.V., Nasluzov, V.A., and Rösch, N., *J. Am. Chem. Soc.*, 2005, vol. 127, p. 11 652.
12. Lee, S., Fan, C., Wu, T., and Anderson, S.L., *Surf. Sci.*, 2005, vol. 578, p. 5.
13. Noguera, C., *J. Phys.: Condens. Matter*, 2000, vol. 32, p. 376.
14. Soares, E.A., van Hove, M.A., Wallers, C.F., and McCarty, K.F., *Phys. Rev. B: Condens. Matter*, 2002, vol. 65, p. 195 405.
15. Rivanenkov, V.V., Nasluzov, V.A., Shor, A.M., Neyman, K.M., and Rösch, N., *Surf. Sci.*, 2003, vol. 525, p. 173.
16. Nasluzov, V.A., Shulimovich, T.V., Shor, A.M., Bukhtiyarov, V.I., and Rösch, N., *Phys. Status Solidi B*, 2010, vol. 247, p. 1023.
17. Inntam, C., Moskaleva, L.V., Neyman, K.M., Nasluzov, V.A., and Rösch, N., *Appl. Phys. A*, 2005, vol. 82, p. 181.
18. Neyman, K.M., Inntam, C., Moskaleva, L.V., and Rösch, N., *Chem. Eur. J.*, 2007, vol. 13, p. 277.
19. Inntam, C., Moskaleva, L.V., Yudanov, I.V., Neyman, K.M., and Rösch, N., *Chem. Phys. Lett.*, 2006, vol. 417, p. 515.
20. Nasluzov, V.A., Rivanenkov, V.V., Shor, A.M., Neyman, K.M., and Rösch, N., *Chem. Phys. Lett.*, 2003, vol. 374, p. 487.
21. Hansen, K.R., Worren, T., Stanpel, S., Lœgsgaard, K., Bäumer, M., Freund, H.-J., Besenbacher, F., and Stensgaard, I., *Phys. Rev. Lett.*, 1999, vol. 83, p. 4120.
22. Phala, N.S., Klatt, G., and van Steen, E., *Chem. Phys. Lett.*, 2004, vol. 395, p. 33.
23. Wang, J., Wang, G., and Zhao, J., *Phys. Rev. B: Condens. Matter*, 2003, vol. 66, p. 035418.
24. Cai, S.-H., Neyman, K.M., Hu, A., and Rösch, N., *J. Phys. Chem. B*, 2000, vol. 104, p. 11 506.
25. Neyman, K.M., Rösch, N., and Pacchioni, G., *Appl. Catal., A*, 2000, vol. 191, p. 3.
26. Ivanova-Shor, E.A., Nasluzov, V.A., Shor, A.M., Vayssilov, G.N., and Rösch, N., *J. Phys. Chem. C,* 2007, vol. 111, p. 12 340.
27. Antonietti, J.-M., Mickalski, M., Heiz, U., Jones, H., Lim, K.H., Rösch, N., Del Vitto, A., and Pacchioni, G., *Phys. Rev. Lett.,* 2005, vol. 94, p. 213 402.
28. Del Vitto, A., Pacchioni, G., Lim, K.H., Rösch, N., Antonietti, J.-M., Mickalski, M., Heiz, U., and Jones, H., *J. Phys. Chem. B*, 2005, vol. 109, p. 19876.
29. Berden, G., Peeters, R., and Meijer, G., *Int. Rev. Phys. Chem.*, 2000, vol. 19, p. 565.
30. Scherer, J.J., Paul, J.B., O'Keefe, A., and Saykally, J.R., *Chem. Rev.*, 1997, vol. 97, p. 25.
31. Lim, K.H., Shor, A.M., Zakharieva, O., and Rösch, N., *Chem. Phys. Lett.*, 2007, vol. 444, p. 280.
32. Li, F., Yu, P., Hartl, M., Daemen, L.L., Eckert, J., and Gates, B.C., *Z. Phys. Chem.*, 2006, vol. 220, p. 1553.
33. Vayssilov, G.N., Gates, B.C., and Rösch, N., *Angew. Chem., Int. Ed. Engl.*, 2003, vol. 42, p. 1391.
34. Vayssilov, G.N. and Rösch, N., *Phys. Chem. Chem. Phys.*, 2005, vol. 7, p. 4019.
35. Ponec, V., *Appl. Catal., A,* 1997, vol. 149, p. 27.
36. Gallezot, P. and Richard, D., *Catal. Rev. Sci. Eng.*, 1998, vol. 40, p. 81.
37. Claus, P., *Top. Catal.*, 1998, vol. 5, p. 51.
38. Bron, M., Teschner, D., Knop-Gericke, A., Steinhauer, B., Scheybal, A., Hävecker, M., Wang, D., Födisch, R., Hönicke, D., Wootsch, A., Schlögl, R., and Claus, P., *J. Catal.*, 2005, vol. 234, p. 37.
39. Bron, M., Teschner, D., Knop-Gericke, A., Jentoft, F.C., Kröhnert, J., Hohmeyer, J., Volckmar, C., Steinhauer, B., Schlögl, R., and Claus, P., *Phys. Chem. Chem. Phys.*, 2007, vol. 9, p. 3559.
40. Bron, M., Teschner, D., Wild, U., Steinhauer, B., Knop-Gericke, A., Volckmar, C., Wootsch, A., Schlögl, R., and Claus, P., *Appl. Catal., A*, 2008, vol. 341, p. 127.
41. Mohammad, A.B., Lim, K.H., Yudanov, I.V., Neyman, K.M., and Rösch, N., *Phys. Chem. Chem. Phys.*, 2007, vol. 9, p. 1247.
42. Mohammad, A.B., Yudanov, I.V., Lim, K.H., Neyman, K.M., and Rösch, N., *J. Phys. Chem. C*, 2008, vol. 112, p. 1628.
43. Ledentu, V., Dong, W., and Sautet, P., *Surf. Sci.*, 1998, vol. 413, p. 518.
44. Xu, Y., Greeley, J., and Mavrikakis, M., *J. Am. Chem. Soc.*, 2005, vol. 127, p. 12823.
45. Lim, K.H., Mohammad, A.B., Yudanov, I.V., Neyman, K.M., Bron, M., Claus, P., and Rösch, N., *J. Phys. Chem. C*, 2009, vol. 113, p. 13231.
46. Lim, K.H., Chen, Z.-X., Neyman, K.M., and Rösch, N., *Chem. Phys. Lett.*, 2006, vol. 420, p. 60.
47. Loffreda, D., Delbecq, F., Vigné, F., and Sautet, P., *Angew. Chem., Int. Ed. Engl.*, 2005, vol. 44, p. 5279.
48. Loffreda, D., Delbecq, F., Vigné, F., and Sautet, P., *J. Am. Chem. Soc.*, 2006, vol. 128, p. 1316.
49. Holladay, J.D., Wang, Y., and Jones, E., *Chem. Rev.*, 2004, vol. 104, p. 4767.

50. Usami, Y., Kagawa, K., Kawazoe, M., Matsumura, Y., Sakurai, H., and Haruta, M., *Appl. Catal., A*, 1998, vol. 171, p. 123.
51. Shiozaki, R., Hayakawa, T., Liu, Y.Y., Ishii, T., Kumagai, M., Hamakawa, S., Suzuki, K., Itoh, T., Shishido, T., and Takehira, K., *Catal. Lett.*, 1999, vol. 58, p. 131.
52. Schauermann, S., Hoffmann, J., Johánek, V., Hartmann, J., Libuda, J., and Freund, H.-J., *Angew. Chem., Int. Ed. Engl.*, 2002, vol. 41, p. 2532.
53. Morkel, M., Kaichev, V.V., Rupprechter, G., Freund, H.-J., Prosvirin, I.P., and Bukhtiyarov, V.I., *J. Phys. Chem. B*, 2004, vol. 108, p. 12 955.
54. Borasio, M., Rodríguez de la Fuente, O., Rupprechter, G., and Freund, H.-J., *J. Phys. Chem. B*, 2005, vol. 109, p. 17 791.
55. Rodríguez de la Fuente, O., Borasio, M., Galletto, P., Rupprechter, G., and Freund, H.-J., *Surf. Sci.*, 2004, vols. 566–568, p. 740.
56. Yudanov, I.V., Matveev, A.V., Neyman, K.M., and Rösch, N., *J. Am. Chem. Soc.*, 2008, vol. 130, p. 9342.
57. Yudanov, I.V., Sahnoun, R., Neyman, K.M., and Rösch, N., *J. Chem. Phys.*, 2002, vol. 117, p. 9887.
58. Yudanov, I.V., Sahnoun, R., Neyman, K.M., Rösch, N., Hoffmann, J., Schauermann, S., Johánek, V., Unterhalt, H., Rupprechter, G., Libuda, J., and Freund, H.-J., *J. Phys. Chem. B*, 2003, vol. 107, p. 255.
59. Yudanov, I.V., Neyman, K.M., and Rösch, N., *Phys. Chem. Chem. Phys.*, 2006, vol. 8, p. 2396.
60. Yudanov, I.V., Metzner, M., Genest, A., and Rösch, N., *J. Phys. Chem. C*, 2008, vol. 112, p. 20269.
61. Teschner, D., Vass, E., Hävecker, M., Zafeiratos, S., Schnörch, P., Sauer, H., Knop-Gericke, A., Schlögl, R., Chamam, M., Wootsch, A., Canning, A.S., Gamman, J.J., Jackson, S.D., McGregor, J., and Gladden, L.F., *J. Catal.*, 2006, vol. 242, p. 26.
62. Teschner, D., Borsodi, J., Wootsch, A., Révay, Z., Hävecker, M., Knop-Gericke, A., Jackson, S.D., and Schlögl, R., *Science*, 2008, vol. 320, p. 86.
63. Wilde, M., Fukutani, K., Ludwig, W., Brandt, B., Fischer, J.H., Schauermann, S., and Freund, H.-J., *Angew. Chem., Int. Ed. Engl.*, 2008, vol. 47, p. 9289.
64. Teschner, D., Révay, Z., Borsodi, J., Hävecker, M., Knop-Gericke, A., Schlögl, R., Milroy, D., Jackson, S.D., Torres, D., and Sautet, P., *Angew. Chem., Int. Ed. Engl.*, 2008, vol. 47, p. 9274.
65. Neyman, K.M., Inntam, C., Gordienko, A.B., Yudanov, I.V., and Rösch, N., *J. Chem. Phys.*, 2005, vol. 122, p. 174 705.
66. Yudanov, I.V., Neyman, K.M., and Rösch, N., *Phys. Chem. Chem. Phys.*, 2004, vol. 6, p. 116.
67. Viñes, F., Loschen, C., Illas, F., and Neyman, K.M., *J. Catal.*, 2009, vol. 266, p. 59.
68. Kozlov, S.M., Yudanov, I.V., Aleksandrov, H.A., and Rösch, N., *Phys. Chem. Chem. Phys.*, 2009, vol. 11, p. 10955.